Nanoscale

PAPER

View Article Online
View Journal | View Issue

Cite this: *Nanoscale*, 2024, **16**, 17868

Click catalysis and DNA conjugation using a nanoscale DNA/silver cluster pair†

Caleb J. Setzler and Jeffrey T. Petty *

DNA-bound silver clusters are most readily recognized by their strong fluorescence that spans the visible and near-infrared regions. From this suite of chromophores, we chose a green-emitting Ag_{10}^{6+} bound to $C_4AC_4TC_3GT_4$ and describe how this DNA/cluster pair is also a catalyst. A DNA-tethered alkyne conjugates with an azide *via* cycloaddition, an inherently slow reaction that is facilitated through the joint efforts of the cluster and DNA. The Ag_{10}^{6+} structure is the catalytic core in this complex, and it has three distinguishing characteristics. It facilitates cycloaddition while preserving its stoichiometry, charge, and spectra. It also acidifies its nearby alkyne to promote H/D exchange, suggesting a silver–alkyne complex. Finally, it is markedly more efficient when compared with related multinuclear DNA–silver complexes. The Ag_{10}^{6+} is trapped within its $C_4AC_4TC_3GT_4$ host, which governs the catalytic activity in two ways. The DNA has orthogonal functional groups for both the alkyne and cluster, and these can be systematically separated to quench the click reaction. It is also a polydentate ligand that imprints an elongated shape on its cluster adduct. This extended structure suggests that DNA may pry apart the cluster to open coordination sites for the alkyne and azide reactants. These studies indicate that this DNA/silver cluster pair work together with catalysis directly driven by the silver cluster and indirectly guided by the DNA host.

Received 15th July 2024,
Accepted 22nd August 2024

DOI: 10.1039/d4nr02938k

rsc.li/nanoscale

Introduction

Size dictates the chemical and optical properties of noble metal nanomaterials, with distinctive behaviors emerging at nanometer scales.[1] For example, while gold in its bulk form is inert, its nanoparticles catalyze CO oxidation with a sharp 100-fold jump in efficiency for sizes $\lesssim$6 nm.[2,3] These small nanoparticles are active because large surface areas expose coordination sites for exogenous reagents.[4] This surface chemistry and catalysis are now more precisely controlled using noble metal nanoclusters.[5,6] These are more precisely described as nanoscale molecules because they have a well-defined number of metals and ligands, organized as a metal core in a ligand shell.[7] Now, size becomes a less relevant metric, and the stoichiometry, structure, charge, and coordination environment dictate catalytic efficiency.[8] Their catalysis is being studied and optimized through a fruitful collaboration of experimental and theoretical studies. A suite of synthetic methods can manipulate both the metal core and ligand shell at the atomic level.[9] X-ray diffraction along with a diverse set of analytical tools can atomically map these complexes.[10] High-level theoretical calculations are used to develop models to understand and optimize catalysis.[11] Here, we describe a nanoscale molecule comprised of a silver cluster within DNA, and this complex collectively catalyzes a cycloaddition reaction.

Transition metal cations are the linchpins of alkyne–azide cycloadditions because they catalyze these click reactions with rates that are 10^7–10^8 faster than the original Huisgen reaction.[12–15] These catalyzed reactions are efficient at room temperature and in dilute solutions and are consequently used to link modular units and synthesize novel nanomaterials.[16–19] A metal center facilitates stepwise annulation by coordinating an alkyne and azide in its open sites.[20] This metal also activates these pendant ligands because it is an electrophile. For example, Cu^+ coordinates across alkyne π-bonds to withdraw electron density and acidify the terminal proton.[15] A nucleophilic acetylide then attacks its neighboring azide, and the resulting C–N bond sets the foundation for an eventual triazole ring closure.[13] While a single Cu^+ facilitates alkyne–azide cycloadditions, multinuclear complexes are more efficient. Two copper coordination sites are supported by kinetic studies that establish a second-order rate law with respect to copper.[21] A dimeric Cu(I) catalyst is supported because a copper acetylide assembles with a Cu(I) complex and exchanges ^{63}Cu and ^{65}Cu isotopes.[22] The pendant ligands freely migrate between the two coordination centers. The diverse end-on and side-on coordination modes of copper acetylides may underlie this enhanced activity because these interlinked complexes readily evolve into copper-triazole intermediates.[23–25] To precisely

Department of Chemistry, Furman University, Greenville, SC, 29613, USA.
E-mail: jeff.petty@furman.edu

† Electronic supplementary information (ESI) available. See DOI: https://doi.org/10.1039/d4nr02938k

control metal stoichiometry, molecular and nanoscale complexes have been synthesized.

Click reactions are widely used because they can be adapted and optimized for diverse reaction conditions, so these 'black box' approaches have motivated the search for more precisely defined catalysts.[19,26–28] For example, di-nuclear Cu^+ complexes are bridged by a bidentate carbene and labile acetate, and these complexes are effective homogeneous catalysts in a range of solvents.[29] Larger nanoscale molecules offer new opportunities to explore the metal stoichiometry, structure, and coordination environment. One such nanocluster complex incorporates eight Cu^+ that are internally linked by acetylides and peripherally capped by carbenes.[30] The acetylides link copper atoms *via* both σ and π bonds, and the complex fluctuates with rapidly exchanging ligands. A Cu_{20} complex is concentrically organized around a partially reduced Cu_4^{2+} core with an outer shell having 12 acetylide ligands bridging 16 Cu^+.[31] The acetylides chemically exchange with exogenous alkynes to yield a mixture of triazole products. A Cu_{58} cluster is a click catalyst whose activity is enhanced by excising a single copper atom.[32] This Cu_{57} may be more active because the copper atoms and ligands around the vacated site reorganize. Mixed Au/Cu and Ag/Cu clusters reveal that electronic synergism facilitates alkyne/azide annulations.[33,34]

Besides Cu(I), other transition metals catalyze click reactions, and we consider a silver molecule.[13,35,36] Again highlighting size-dependent properties, these molecular forms of silver are fluorophores that are $\sim 10^{10}$ and $\sim 10^{2}$ brighter than bulk and nanoparticle forms of silver, respectively.[37,38] These fluorophores have diverse spectra that have been revealed using DNA.[39] Single-stranded oligonucleotides coordinate silvers via their electron-rich, heterocyclic nucleobases, and multiple nucleobases frame binding pockets for a specific multinuclear cluster. DNA is programmable because its sequence and structure encode specific chromophores with spectra that span the visible and near-infrared regions and brightnesses that vary by $\sim 10^{3}$.[40,41] Here, we consider this spectroscopic DNA code from a chemical perspective. Silver clusters are protected within their DNA shell, but this matrix is permeable, as illustrated by cluster reactions with oxidizing and reducing agents.[42–45] Here, we study a DNA/silver cluster pair that catalyzes alkyne–azide cycloadditions, a favored and selective reaction that is not perturbed by the diverse functional groups in DNA.[46] We first describe the DNA scaffold that shares both a silver cluster and an alkyne. The DNA-tethered alkyne reacts with azides without changing the nearby cluster, and a covalent triazole linkage was confirmed by etching the cluster from its DNA matrix. The cluster/DNA complex in D_2O reveals that the cluster acidifies its neighboring alkyne, possibly *via* a silver–alkyne complex. The click reaction efficiency depends on the cluster–alkyne proximity, which was controlled by inserting thymine spacers in the DNA strand. The solution pH also regulates the reaction efficiency. Collectively, these experiments show how a DNA/silver cluster pair work together to catalyze alkyne–azide cycloadditions.

Experimental

Synthesis

The desalted oligonucleotides $C_4AC_4TC_3GT_4$ and Hx-$C_4AC_4TC_3GT_4$, where Hx is 1-hexyne attached at the 5′ phosphate position, were purchased from Integrated DNA Technologies and dissolved in deionized water before use. Molar extinction coefficients were calculated based on the nearest-neighbor approximation,[47] and the concentrations of these DNA stock solutions were determined using the Lambert–Beer law. In a typical synthesis, 150 μL of sodium cacodylate buffer solution (1 mM, pH = 7) that contained 30 μM $C_4AC_4TC_3GT_4$ (**1**) and 300 μM $AgNO_3$ (10 molar equivalents : **1**) was used. The mixture was first heated (~80 °C) for 5 min and then cooled to room temperature. Then an aqueous solution of $NaBH_4$ was added (5 molar equivalents : **1**) and vortexed. The buffers were acetic acid/acetate (pH = 5), cacodylic acid/cacodylate (pH = 6–7), and boric acid/borate (pH = 7.5 and 8). The azides were N_3–C_3H_6–NH_2, N_3–$C_6H_{12}O_2$–$C_{10}H_{16}N_3O_2S$ (Lumiprobe) and N_3–C_3H_6–OH (Synthonix). D_2O (Cambridge Isotopes) was used for H/D exchange.

Optical characterization

Absorption spectra of DNA–Ag cluster conjugates were collected on a Cary 50 UV-Vis spectrophotometer (Varian), and steady-state emission spectra were collected on a Fluoromax-3 spectrofluorometer (Jobin–Yvon Horiba). Fluorescence quantum yields (QY) were measured by following well-established protocols using fluorescein as the standard (QY = 95%).[48] Time-correlated single-photon counting measured the fluorescence lifetimes and anisotropies of these nanoclusters. Samples were excited by a pulsed 470 nm laser (PicoQuant) at a rate of 20 MHz using a FluoTime 300 (PicoQuant) photoluminescence spectrometer. The excitation beam was vertically polarized, and its power was fine-tuned to achieve a detection rate of fewer than 5 photons per 100 pulses ($<5 \times 10^5$ Hz). The emission was collected at right-angled geometry with the emission polarizer set to the magic angle (~55°), and spectrally filtered using the monochromator. The instrument response function (IRF) was collected using colloidal silica (Aldrich), and the FWHM of the IRF was ~150 ps. The kinetics of fluorescence decay was extracted through IRF reconvolution fitting of the measured decay (EasyTau). Fluorescence anisotropy measurements were conducted using vertically (V) polarized excitation along with vertically (V) or horizontally (H) polarized emission.[49] The *G*-factor accounts for the detection efficiency of vertically and horizontally polarized emission and was measured using fluorescein. The fluorescence decays under two different configurations, $I_{VV}(t)$ and $I_{VH}(t)$, were reconvolved with the IRF to calculate the anisotropy decay, $r(t)$, and rotational correlation time, τ_c (EasyTau).

Mass spectrometry

The stoichiometry and charge of DNA–Ag cluster conjugates were characterized by electrospray ionization mass spec-

trometry (Q-TOF G2-S, Waters). DNA–silver clusters were dialyzed to remove low molecular weight impurities such as Na^+. The samples were diluted with 100× volumes of 1 mM ammonium acetate and then reconcentrated by centrifugal dialysis using2 kDa cutoff filters (VivaSpin 20). The samples were diluted to ~0.3 μM with 1 mM ammonium acetate and then infused *via* a syringe pump operated at 20 μL min^{-1}. The spectra were collected in the negative ion mode with a capillary voltage of −2.7 kV, a sampling cone voltage of −15 V, an extraction cone voltage of 10 V, a cone gas flow of 45 L h^{-1}, and a desolvation gas flow of 450 L h^{-1}. The source temperature was 80 °C, and the desolvation temperature was 150 °C. Mass calibration was performed using aggregates of sodium iodide in the 400 < m/z < 2000 range. The spectra were analyzed using MassLynx V4.1.

Results

Neighbors in the shared DNA scaffold

$C_4AC_4TC_3GT_4$ (**1**) assembles a silver cluster and alkyne *via* two distinct binding sites (Fig. 1A). This sequence was chosen because it selectively forms a single silver chromophore with $\lambda_{ex}/\lambda_{em}$ = 490/555 nm, and its multidentate binding site has been characterized by varying the DNA sequence (Fig. 1B).[50] The four thymine spacers at the 3′ terminus can be removed; however, shorter variants of $C_4AC_4TC_3G$ no longer favor the green emitting cluster, indicating that this 14-nucleobase tract is the minimal, core-binding site.[43,50–52] This sequence folds around the cluster with the central thymine functioning as a hinge.[49] The DNA was further modified with a 1-hexyne molecule at its 5′ phosphate position, and this covalently modified strand is henceforth referred to as **Hx-1**. In summary, $C_4AC_4TC_3GT_4$ (**1**) is a scaffold that shares an alkyne and a green-emitting silver cluster. The cluster is a silver molecule that was characterized using its mass and optical spectra.

Hx-1 mimicked **1** because it formed the same silver molecule, whose stoichiometry and charge were measured by electrospray ionization mass spectrometry (Fig. 1C, 1S and Table 1S†). As with the parent strand, **Hx-1** was combined with Ag^+ ions, which were chemically reduced to yield a range of adducts with 4–10 silvers. Ag_{10} dominated, and it is a charged adduct that partially neutralizes the DNA.[38,49,50,53] **Hx-1**/Ag_{10} complexes with net −4 and −5 charges were identified, each with characteristic isotopic distributions due to the 51.8% ^{107}Ag : 48.2% ^{109}Ag mixture in naturally occurring silver (Fig. 1C-inset and 1S†). The m/z values and the intensities of 49 isotopologue peaks were analyzed to yield the molecular formulas $[(C_{175}H_{221}N_{53}O_{113}P_{18})^{-10}(Ag_{10})^{6+}]^{-4}$ and $[(C_{175}H_{220}N_{53}O_{113}P_{18})^{-11}(Ag_{10})^{6+}]^{-5}$ (Table 1S†).[53] Without the silver adduct, the −4 and −5 charged strands alone would have H_{227} and H_{226}, respectively, so each complex is missing 6 H^+. The reason for this deficit lies with the phosphate backbone. It acts like a buffer because its H^+ ions are labile and displaced by the cationic silver cluster. The 6 fewer H^+ ions suggests that the cluster is Ag_{10}^{6+}. Both ions had Ag_{10}^{6+} adducts, consistent with a cluster that dictates protonation of the phosphate backbone. Oxidation states of other DNA-bound silver clusters have been measured by both mass spectrometry in the gas phase and XANES measurements in solution, yielding the same charge.[54] Based on its +6 oxidation state, the Ag_{10}^{6+} has 4 Ag^0 atoms, which are responsible for its green fluorescence.[55] The optical spectra are described next.

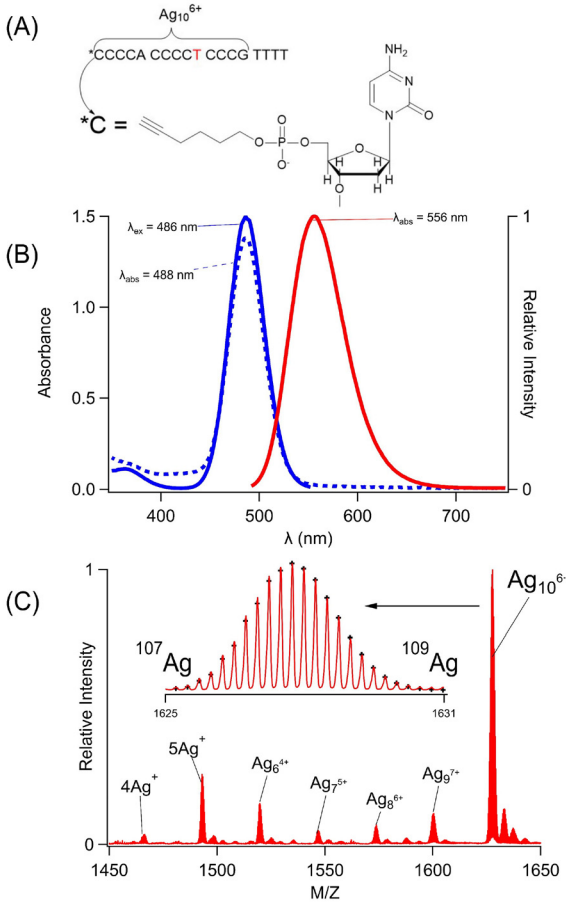

Fig. 1 (A) The model of Hx-$C_4AC_4TC_3GT_4$ with 1-hexyne attached at the 5′ phosphate (**Hx-1**) position and Ag_{10}^{6+} bound to the $C_4AC_4TC_3G$ sub-sequence. The central T highlighted in red emphasizes a folding site. (B) Absorption (dotted blue), excitation (solid blue), and emission (solid red) spectra of Ag_{10}^{6+} bound to $C_4AC_4TC_3GT_4$. Coincidence of the absorption and excitation spectra suggests that a single cluster forms. (C) Mass spectra of the −4 state of **Hx-1** with its Ag adducts. The dominant species is Ag_{10}^{6+}. The inset shows the ^{107}Ag : ^{109}Ag isotopic distribution, by which the molecular formula was determined.

The coordination environment in **Hx-1** was further interrogated using the absorption and fluorescence spectra of the Ag_{10}^{6+} adduct. This chromophore is a sensitive reporter because it has diverse spectra, ranging from a weakly emissive, λ_{max} = 400 nm chromophore to a 60-fold brighter, λ_{max} = 490 nm fluorophore.[56,57] Given these large changes, the Ag_{10}^{6+} spectra can discern differences between the **1** and **Hx-1** hosts (Fig. 2S†). The absorption spectra have similar λ_{max} values and absorbances, thus indicating that the clusters reside in comparable binding sites and form with similar efficiencies.

The absorption and excitation maxima overlap, suggesting that a single cluster develops within their respective binding sites. The emission spectra have the same λ_{max} = 556 nm, and the fluorescence quantum yields are similar being 24 ± 4% for **1**/Ag_{10}^{6+} and 30 ± 4% for **Hx-1**/Ag_{10}^{6+}. The respective intensity-weighted average fluorescence lifetimes are 2.05 ± 0.03 ns and 2.23 ± 0.04 ns, again supporting similar electronic environments. The fluorescence decays were further utilized to compare the shapes of the DNA–cluster complexes. During fluorescence relaxation, the emission depolarizes as the complexes rotate to yield rotation correlation times of 2.50 ± 0.05 ns and 2.64 ± 0.09 ns using the strands without and with the hexyne, respectively. These times are similar to the heterodimeric (C_4AC_4T + C_3GT_4)/Ag_{10}^{6+} complex and suggests that both **Hx-1** and **1** are folded at the central thymine.[49,58] Thus, the mass and optical spectra demonstrate that the same Ag_{10}^{6+} fluorophore forms with both **Hx-1** and **1**.

Catalytic cluster

The Ag_{10}^{6+} and hexyne are nearby in their shared DNA scaffold and yet appear to be decoupled, as the same Ag_{10}^{6+} adduct has nearly identical spectra using $C_4AC_4TC_3GT_4$ without and with 1-hexyne appended. However, from the vantage of the alkyne, it now reacts with azides, a reaction that is prohibitively slow without the cluster.[12] Two smaller aliphatic and one larger biotin-based azides were used: N_3–C_3H_6–NH_2, N_3–C_3H_6–OH, and N_3–$C_6H_{12}O_2$–$C_{10}H_{16}N_3O_2S$ (biotin) (Fig. 2A, B, and 3S†). Azide complexes with **Hx-1**/Ag_{10}^{6+} were identified in the mass spectra, and their formulas were derived from the isotopologue peaks in the −4 and −5 states of these complexes. Based on the *m*/*z* values and the isotopologue intensity distributions, the following formulas were derived for the −4 and −5 charged ions of each complex: $[(C_{178}H_{229}O_{113}N_{57}P_{18})^{-10}(Ag_{10})^{6+}]^{-4}$ and $[(C_{178}H_{228}O_{113}N_{57}P_{18})^{-11}(Ag_{10})^{6+}]^{-5}$ for N_3–C_3H_6–NH_2 (Table 2S†), $[(C_{178}H_{228}O_{114}N_{56}P_{18})^{-10}(Ag_{10}^{6+})]^{-4}$ and $[(C_{178}H_{227}O_{114}N_{56}P_{18})^{-11}(Ag_{10}^{6+})]^{-5}$ for N_3–C_3H_6–OH (Table 3S†), and $[(C_{191}H_{249}O_{117}N_{59}SP_{18})^{-10}(Ag_{10}^{6+})]^{-4}$ and $[(C_{191}H_{248}O_{117}N_{59}SP_{18})^{-11}(Ag_{10}^{6+})]^{-5}$ for N_3–$C_6H_{12}O_3$–biotin (Table 4S†). These formulas show Ag_{10}^{6+} is preserved when the DNA-tethered hexyne reacts with the azides. Furthermore, the coordination sites are conserved, as indicated in similar absorption spectra (Fig. 4S†). Our subsequent results focus on N_3–C_3H_6–NH_2. While **Hx-1** hosts other silver adducts, only the **Hx-1**/Ag_{10}^{6+} complex associates with this azide, and the efficiency of labelling was calculated by integrating peak areas for all DNA/silver complexes (Fig. 2C, red *vs.* black peaks). The integrity of the N_3–C_3H_6–NH_2/DNA/cluster complex was challenged by diluting a sample with 100× volumes of solution to dissociate weakly bound complexes and then reconcentrated using centrifugal dialysis. The absorption spectra remain consistent with the same λ_{max} and absorbance, indicating that the cluster is stable in its azide-tagged DNA host (Fig. 5S†). Also, the reaction efficiencies are similar, so we conclude that only the DNA-bound Ag_{10}^{6+}, and not leached Ag^0/Ag^+, facilitate the reaction (Fig. 5S†).[31,59] Thus, the DNA-bound cluster facilitates but remains unchanged by alkyne–azide coupling.

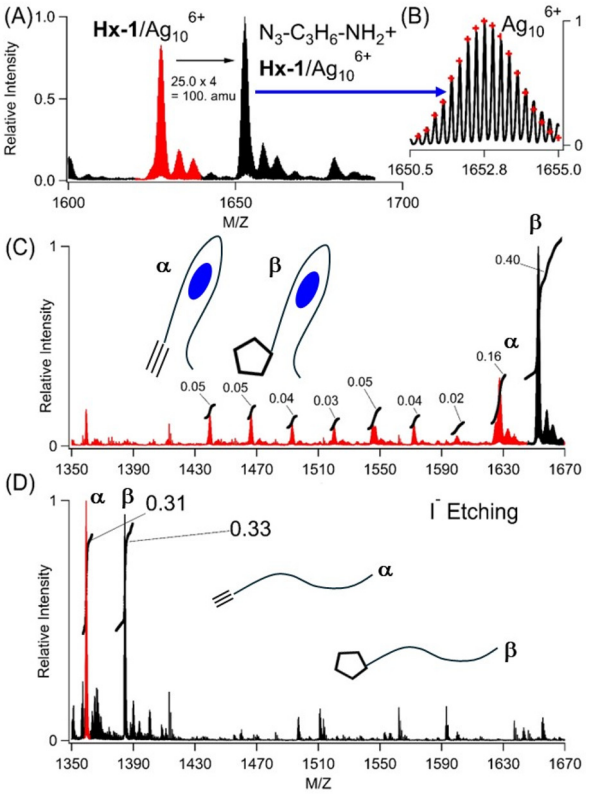

Fig. 2 (A) Mass spectra of the −4 charged ion of **Hx-1**/Ag_{10}^{6+} (red) after reacting with N_3–C_3H_6–NH_2 to form a new complex with the expected mass difference of 100 amu (black). (B) Expanded view of the **Hx-1**/Ag_{10}^{6+}/N_3–C_3H_6–NH_2 isotopic distribution by which the molecular formula was determined (see Table 2S†). (C) Mass spectra of **Hx-1**/Ag_{10}^{6+} (red peak, α label) and **Hx-1**/Ag_{10}^{6+}/N_3–C_3H_6–NH_2 (black peak, β label) before etching. Relative integrated areas are included, and these were used to calculate the labelling efficiency of **Hx-1**/Ag_{10}^{6+}/N_3–C_3H_6–NH_2 *vs.* all the other DNA/silver complexes. (D) Mass spectra of **Hx-1** (red peak, α label) and **Hx-1**/N_3–C_3H_6–NH_2 (black peak, β label) after etching. The relative integrated peak areas are included. The *m*/*z* ranges match in (C) and (D) to emphasize that silver atoms are removed from DNA using I^-.

Ag_{10}^{6+} was used as a starting point to create other possible silver-laden DNA catalysts.[44] This chromophore has 4 Ag^0 atoms that provide a photochemical handle by which Ag_{10}^{6+} can be selectively excited and degraded by irradiating at 490 nm.[44] The photodestruction quantum yield was ~10^{-4}, so the sample was irradiated for an extended period. As the Ag_4^0 absorption at 490 nm diminished, a new higher energy transition due to Ag_2^0 developed at 340 nm (Fig. 6SC†).[60–64] However, this photochemical change is more interesting than a simple $Ag_4^0 \rightarrow Ag_2^0$ conversion because the mass spectra identified two distributions of photoproducts (Fig. 6SA and 6SB†). As expected from the λ = 490 → 340 nm shift, the DNA coordinated to Ag_2^0, but multiple clusters with different numbers of Ag^+ were identified – Ag_6^{4+}, Ag_7^{5+} (dominant species), Ag_8^{6+}, and Ag_9^{7+}. Irradiation also produced purely oxidized 4 and 5 Ag^+ adducts, which are devoid of Ag^0 and thus spectrally silent. We used a sample irradiated for a short time

to collectively evaluate how the DNA-bound Ag^+, Ag_2^0, and Ag_4^0 species react with N_3–C_3H_6–NH_2. Despite their high abundance and redundancy, the Ag^+ and Ag_2^0 complexes did not react and only the Ag_{10}^{6+} adduct promoted alkyne–azide coupling (see red peaks in Fig. 6SA†). Thus, the alkyne reaction with azides is specific for Ag_{10}^{6+}, and the reaction products were characterized by extracting the cluster from the DNA.

Three experiments indicate that Ag_{10}^{6+} facilitates cycloaddition to yield a covalently linked triazole, as shown using N_3–C_3H_6–NH_2 with **Hx-1**/Ag_{10}^{6+}. First, this azide remained integrated with the DNA after Ag_{10}^{6+} was removed. Silver clusters were etched by I^-, presumably because AgI(s) has such a small $K_{sp} = 10^{-18}$. With 1 equivalent of iodide : silver, the Ag_{10}^{6+} absorption at 490 nm was quenched, signalling that silvers were no longer associated with the DNA (Fig. 7S†). In support of this, two strands devoid of silvers emerged in the mass spectra: **Hx-1** alone and with N_3–C_3H_6–NH_2 (Fig. 2C). The latter supports alkyne–azide cycloaddition between the DNA-tethered alkyne and N_3–C_3H_6–NH_2, a union that is selective and strongly thermodynamically favored ($\Delta G \sim -45$ kcal).[12,16] The areas of these two peaks were integrated to give a labelling efficiency of 52%, comparable to the value of 48% before etching (Fig. 2D *vs.* 2C). Inactive DNA-bound Ag^+ and Ag_2^0 adducts were further supported by the low labelling efficiency of a photolyzed sample (Fig. 8SB†). Second, N_3–C_3H_6–NH_2 was added to **1**/Ag_{10}^{6+} but did not form a stable complex (Fig. 9S†). Third, after reaction with N_3–C_3H_6–NH_2 and then I^-, the denuded DNA strands were dialyzed against 100× and 10 000× volumes of solution (Fig. 10S†). The relative amounts of unlabelled and labelled DNA did not change, further supporting a stable, covalently linked triazole.

Enhanced acidity

Hx-1 becomes more acidic due to its Ag_{10}^{6+} adduct, and the acidic site was identified using H/D exchange. The DNA/cluster complex has nearly identical absorption spectra in H_2O and D_2O, suggesting that the clusters were formed with similar efficiencies in the same coordination environment (Fig. 11S†). To isolate the effect of the cluster, it was extracted from its DNA host using CN^-, which readily complexes with Ag^+ to form $Ag(CN)_2^-$. With $K = 10^{18}$, this CN^- and its $Ag(CN)_2^-$ complex ion are expected to overwhelm any affinity of DNA for silvers, as supported by quenched Ag_{10}^{6+} absorption (Fig. 11S†). This sample was finally washed with 100 volumes of H_2O (Fig. 3A – case I). Swapping D_2O with this large amount of H_2O will reprotonate the plethora of naturally acidic and basic functional groups in a DNA strand.[47] However, the alkyne appended onto **1** is inherently more basic with $pK_a \sim 26$, thus resisting reprotonation.[12] Mass spectra show denuded strands with net −5, −4, and −3 charges, and the *m*/*z* values and the isotope distributions of the isotopologue peaks show that the molecular formula has exchanged a hydrogen with deuterium, *i.e.* $C_{175}H_{230}\mathbf{D}N_{53}O_{113}P_{18}$ (DNA with zero net charge) (Fig. 3B, 12SA and Table 5S†). Three other experiments firmly established the alkyne deuteration site. First, **Hx-1**/Ag_{10}^{6+} was prepared in H_2O, and the mass spectra show the expected

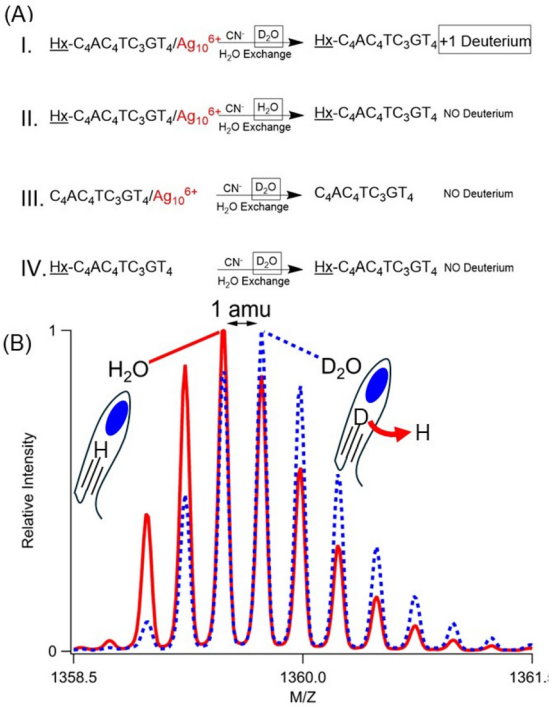

Fig. 3 (A) Reaction conditions used to study deuteration of the alkyne. Complexes were synthesized in either D_2O or H_2O (indicated by boxes). Strands with or without the hexyne (indicated by underlining) and strands with and without the cluster (indicated by red text) were compared. CN^- etched the silver cluster, then samples were washed with H_2O to reprotonate exchangeable sites in the DNA. Denuded strands were then analyzed by mass spectrometry. (B) Mass spectra the −4 charged ion of **Hx-1**/Ag_{10}^{6+} prepared in D_2O (blue dotted lines) and H_2O (red solid lines), etched with CN^-, and washed with H_2O (cases I and II, respectively, above). A shift of 1 amu suggests that the former replaces 1 hydrogen for a deuterium atom.

fully protonated, bare DNA (Fig. 3A – case II, 12SB and Table 6S†). Second, $C_4AC_4TC_3GT_4$/Ag_{10}^{6+} without the hexyne was prepared in D_2O, yet the silver-free DNA was fully protonated (Fig. 3A – case III, 12SC and Table 7S†). As a further control, **Hx-1** without Ag_{10}^{6+} in D_2O shows no deuteration (Fig. 3A – case IV, 12SD and Table 8S†). These experiments suggest that Ag_{10}^{6+} coordinates with and acidifies its neighboring alkyne.

Reaction efficiency

Hx-1 anchors both the cluster and alkyne, and their proximity controls the reaction efficiency. This DNA is modular because it can be lengthened to separate its two adducts. Thymine spacers were inserted because they bind poorly with silvers and do not perturb a cluster coordination site.[51,52] **Hx-T$_x$-1** strands with $x = 0$, 1, 2, 3, and 4 thus hold Ag_{10}^{6+} in its favored $C_4AC_4TC_3G$ binding site while still keeping the hexyne on the 5′ terminus. Considering DNA as a linear polymer, these longer strands progressively distanced the alkyne from its neighboring cluster. All five oligonucleotides formed the same Ag_{10}^{6+} adducts, whose similar $\lambda_{max} \sim 490$ nm and absorbances

suggest that the clusters were developed with comparable efficiencies (Fig. 13S†). Thus, the added thymine spacers were innocuous, and the cluster remained confined and thus progressively more distant from the 5′-terminal hexyne. These DNA/Ag_{10}^{6+} complexes reacted differently with N_3–C_3H_6–NH_2, as the reaction efficiencies were highest without an added thymine (x = 0 strand) but diminished as more thymine spacers were added (Fig. 4 and 14S†). Thus, these results suggest the DNA is modular and can be lengthened to temper the click reaction.

Conditions relevant to click reactions were also considered. Oxidation of redox active metals can render incompetent catalysts.[26,27] With **Hx-1**/Ag_{10}^{6+}, solutions purged with O_2 *vs.* N_2 showed no differences in conversion, suggesting that O_2 does not affect the Ag_{10}^{6+} catalyst (Fig. 15S†).[42] The solution pH can also influence a click reaction through deprotonation of terminal alkynes and reprotonation of Cu-triazolyl intermediates. Over the range from pH = 5–8.5, the same Ag_{10}^{6+} adducts formed with **Hx-1** with little variance in their optical spectra (Fig. 16S and 17S†). However, strong differences emerged with the addition of N_3–C_3H_6–NH_2. The conversion efficiency increases ~25-fold over this pH range, with a sharp jump at pH = 6–7. An enhanced reaction was also observed at higher pH for Cu(I) coordinated with benzimidazole ligands.[65] As with these polydentate amine-based ligands, DNA is a rich reservoir of acidic and basic heteroatoms that may regulate deprotonation and reprotonation steps in a click reaction.[66]

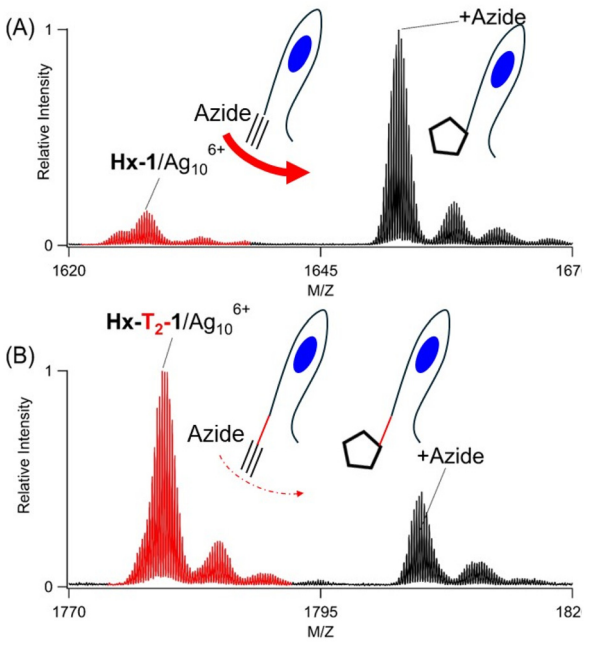

Fig. 4 Mass spectra of the −4 charged ion of **Hx-T_x-1**Ag_{10}^{6+} with x = 0 and 2 (A and B, respectively.). After reaction with N_3–C_3H_6–NH_2, new azide complexes form (black peaks) from their **Hx-T_x-1**/Ag_{10}^{6+} precursors (red peaks). Reaction efficiencies decrease with the number of thymines in the T_x spacers.

Discussion

Together, **Hx-1** and Ag_{10}^{6+} catalyze an alkyne–azide click reaction, and each component in this pair has distinct roles. Ag_{10}^{6+} is the catalyst, and we discuss three of its characteristics – it is preserved while facilitating the click union, it acidifies its neighboring alkyne, and it is distinctly active compared to related complexes. The activity of this catalyst is regulated by the DNA host, which serves two roles – it segregates the cluster within the larger DNA host and it imprints an elongated cluster shape. We now discuss these five characteristics of this nanoscale catalyst.

Ag_{10}^{6+} unites a DNA-tethered alkyne with an azide without changing its stoichiometry, charge, and spectra. However, click reactions conserve atoms, so mass spectra cannot distinguish whether an azide reacts with the alkyne or simply coordinates with silvers. To consider these two possibilities, iodide was added upon completing the reaction. This halide degrades the cluster to quench the Ag_{10}^{6+} absorption and strip the DNA of silvers. Two bare **Hx-1** strands are identified – without and with the azide. With the silver coordination sites now missing, we conclude that the azide is covalently linked as a triazole. In support of this, the **Hx-1**/azide conjugate survives 10 000× dilution, thus supporting a stable, covalent linkage that resists dissociation. Also, without the DNA-bound alkyne, **1**/Ag_{10}^{6+} does not form a stable complex with azides. Thus, Ag_{10}^{6+} catalyzes cycloaddition, and its role as a catalyst is suggested by studies in D_2O.

Transition metals catalyze alkyne–azide cycloadditions in steps, beginning with the deprotonation of a terminal alkyne. Ag_{10}^{6+} may follow a similar catalytic path because it acidifies its neighboring alkyne, thereby effecting the H/D exchange in D_2O. By analogy with other Cu(I) and Ag(I) catalysts, a deprotonated alkyne converts into a metal acetylide, a strong nucleophile that can attack an azide to set the first C–N bond for a triazole.[36,67] Further experiments are underway to evaluate this proposed mechanism.[12] Beyond a mononuclear complex, silver acetylides can be multinuclear with both end-on and side-on coordination to give a rich and diverse array of structures.[25,68] To better understand the nuclearity of the **Hx-1**/Ag_{10}^{6+} catalyst, we studied pared down versions of this complex.

Relative to mononuclear complexes, multinuclear click catalysts are more effective, so smaller analogs of **Hx-1**/Ag_{10}^{6+} were studied. The 4 Ag^0 units in Ag_{10}^{6+} were selectively irradiated to yield DNA complexes with less Ag^0–Ag_2^0 (Ag_6^{4+}, Ag_7^{5+}, Ag_8^{6+}, and Ag_9^{7+}) and purely Ag^+ (3–5 Ag^+) adducts. However, these multinuclear derivatives of Ag_{10}^{6+} are incompetent catalysts, behaving as if the DNA was completely bare. They may be inactive because of their structure. Their wide distribution of silvers suggests that the preexisting **Hx-1** binding site is indiscriminate and has little preference for a particular adduct. Thus, these photoproducts may be loosely bound with ill-defined structures, so they may be poor catalysts. We are searching for truncated oligonucleotides better suited for these photofragments. For example, complementary strands

can shorten long DNA binding sites to favor smaller clusters.[57] Metal oxidation may also underlie the tepid activity of the Ag_2^0 and Ag^+ adducts with **Hx-1**. Dinuclear copper complexes have dynamic coordination environments whose ligands readily exchange because copper oxidation weakens π-backbonding and ligand coordination.[22,69] One avenue to better understand the metal oxidation might be to change the balance of Ag^+ and Ag^0 in a cluster. Specifically, Ag_{11}^{7+} is also a green-emitting fluorophore like Ag_{10}^{6+}, but it has an additional Ag^+ that could alter the activity of this cluster.[32,42,70] We are also studying other DNA/silver cluster complexes. In summary, Ag_{10}^{6+} is the catalytic core of the **Hx-1**/Ag_{10}^{6+} complex and has three characteristics: it joins the alkyne with azides *via* cycloaddition, it acidifies and possibly activates the alkyne, and it is markedly more active than related DNA–silver complexes. The click reaction evolves within the confines of the **Hx-1** scaffold, and we now discuss how it guides these reactions.

The green-emitting Ag_{10}^{6+} exists because it is trapped and shielded inside **Hx-1**, and this $C_4AC_4TC_3G$ coordination site is a discrete unit in a larger DNA polymer. In addition, the DNA was further derivatized with 1-hexyne at its 5′ terminal phosphate position, yielding a dual-labeled **Hx-1**/Ag_{10}^{6+} conjugate. These adducts are independent and were separated by inserting thymine spacers. Furthermore, these binding sites are independent, so the alkyne and cluster adduct can be separated by inserting thymine spacers, neutral spacers that bind poorly with silver. With these longer **Hx-T$_x$-1** strands, the cluster does not spill out of its binding site, as signified by the consistent mass and optical spectra for these variants. As the number of thymine spacers increases, the click conversion efficiency drops. Considering the DNA to be a linear polymer, increasing the distance between the alkyne and the cluster thus tempers the click reaction with azides. Besides phosphates, specific nucleobases can also be alternative sites to derivatize a DNA. For example, X-ray diffraction studies show that the 3′-terminal adenine in $(CACCTAGCGA)_2$-Ag_{16} is not associated with the cluster and can be labeled with peptides and proteins.[71,72] Also, fluorescence anisotropy studies show that the central thymine in $C_4AC_4TC_3GT_4$ (**1**) is a folding site where the strand can be broken.[49] The resulting heterodimer reassembles to form the same green-emitting Ag_{10}^{6+} as the contiguous $C_4AC_4TC_3GT_4$. Thus, we suggest that specific sites could be derivatized in $C_4AC_4TC_3GT_4$/Ag_{10}^{6+} to better understand its click catalysis. DNA is not only a scaffold that tunes the reaction efficiency but is also a polydentate ligand that shapes its cluster adduct.

Bare silver clusters have multiple interconverting isomers, and a DNA strand can select and favor specific isomers. For example, a single-stranded oligonucleotide coordinates a weakly emissive Ag_{10}^{6+} adduct, but this DNA hybridizes with a short complementary strand to now favor a strongly emissive Ag_{10}^{6+}.[56] This switch reverses when the complement denatures. We now consider the shape of the Ag_{10}^{6+} adduct bound to **Hx-1**. This complex is a member of a larger class of Ag_4^0-based chromophores with green emission whose structures have been considered from a variety of perspectives.[38,40,55] EXAFS studies of a DNA-bound Ag_{10}^{6+} show limited metal–metal *vs.* metal–DNA coordination when compared to a related weakly fluorescent cluster.[54,73] UV-based DNA footprinting identifies large segments of the DNA host that are protected from photodegradation by the Ag_{10}^{6+} adduct, again contrasting with localized binding and protection by a weakly fluorescent cluster.[74] Time-resolved infrared spectra show that the $C_4AC_4TC_3GT_4$ strand used in this study chelates with its Ag_{10}^{6+} adduct using multiple nucleobases.[75] X-ray diffraction studies of an Ag_{11}^{7+} unit show a rod-like structure with distinct Ag_6 and Ag_5 subunits that follow the contour of the DNA polymer.[70] Quantum mechanical models predict cluster spectra based on rod-like shapes.[38,55] We propose that Ag_{10}^{6+} bound to **Hx-1** also adopts an elongated shape and is dispersed within its DNA matrix, favoring metal–ligand over metal–metal coordination. An important question is the relative strength of nucleobase–silver coordination and competition with exogenous reagents, and prior studies indicate that reagents can penetrate and access open sites on the cluster.[8,32,44,45]

Conclusion

Single-stranded oligonucleotides encode the spectra of silver molecules *via* their sequence and structure, and this templated synthesis is illustrated by the $C_4AC_4TC_3GT_4$ strand which preferentially forms Ag_{10}^{6+}. Besides being a strong fluorophore with green emission, this cluster also catalyzes click reactions between a DNA-tethered alkyne and azides. We conclude that DNA is a scaffold that guides catalysis in two ways. First, it segregates the cluster into a discrete, orthogonal binding pocket that leaves the larger DNA polymer open to be further functionalized. We hope to probe the nanoscale DNA/cluster catalyst by site-specifically modifying the DNA. Second, DNA imprints the cluster shape and thus prescribes the coordination environment. We hope to modify the DNA polymer to fine-tune how click reagents access open coordination sites and bind with exposed silvers. Our overall conclusion is that silver molecules are effective click catalysts, and their activity can be directed by a DNA scaffold.

Author contributions

Jeffrey Petty and Caleb Setzler contributed equally to this work. Both authors conducted the experiments, analyzed the data, and wrote the manuscript. All authors have read and approved the final version of the manuscript.

Data availability

The data supporting this article are included as part of the ESI.†

Conflicts of interest

No conflicts to declare.

Acknowledgements

The authors thank the National Science Foundation (CHE-1611451 and CHE-2002910) and the Furman Advantage program. This work was supported in part by the National Science Foundation EPSCoR Program under NSF Award No. OIA-1655740. Any opinions, findings, and conclusions or recommendations expressed in this material are those of the author(s) and do not necessarily reflect those of the National Science Foundation.

References

1 P. P. Edwards and J. M. Thomas, *Angew. Chem., Int. Ed.*, 2007, **46**, 5480–5486.
2 M. Haruta, T. Kobayashi, H. Sano and N. Yamada, *Chem. Lett.*, 2006, **16**, 405–408.
3 G. C. Bond and D. T. Thompson, *Gold Bull.*, 2000, **33**, 41–50.
4 N. Lopez, T. V. W. Janssens, B. S. Clausen, Y. Xu, M. Mavrikakis, T. Bligaard and J. K. Nørskov, *J. Catal.*, 2004, **223**, 232–235.
5 M. Brust, M. Walker, D. Bethell, D. J. Schiffrin and R. Whyman, *J. Chem. Soc., Chem. Commun.*, 1994, 801–802, DOI: 10.1039/C39940000801.
6 R. L. Whetten, J. T. Khoury, M. M. Alvarez, S. Murthy, I. Vezmar, Z. L. Wang, P. W. Stephens, C. L. Cleveland, W. D. Luedtke and U. Landman, *Adv. Mater.*, 1996, **8**, 428–433.
7 R. Jin, *Nanoscale*, 2015, **7**, 1549–1565.
8 M. F. Matus and H. Häkkinen, *Nat. Rev. Mater.*, 2023, **8**, 372–389.
9 Y. Du, H. Sheng, D. Astruc and M. Zhu, *Chem. Rev.*, 2020, **120**, 526–622.
10 P. D. Jadzinsky, G. Calero, C. J. Ackerson, D. A. Bushnell and R. D. Kornberg, *Science*, 2007, **318**, 430–433.
11 O. Lopez-Acevedo, K. A. Kacprzak, J. Akola and H. Häkkinen, *Nat. Chem.*, 2010, **2**, 329–334.
12 F. Himo, T. Lovell, R. Hilgraf, V. V. Rostovtsev, L. Noodleman, K. B. Sharpless and V. V. Fokin, *J. Am. Chem. Soc.*, 2005, **127**, 210–216.
13 C. Wang, D. Ikhlef, S. Kahlal, J.-Y. Saillard and D. Astruc, *Coord. Chem. Rev.*, 2016, **316**, 1–20.
14 C. W. Tornøe, C. Christensen and M. Meldal, *J. Org. Chem.*, 2002, **67**, 3057–3064.
15 V. V. Rostovtsev, L. G. Green, V. V. Fokin and K. B. Sharpless, *Angew. Chem., Int. Ed.*, 2002, **41**, 2596–2599.
16 H. C. Kolb, M. G. Finn and K. B. Sharpless, *Angew. Chem., Int. Ed.*, 2001, **40**, 2004–2021.
17 D. Honcharenko, K. Druceikaite, M. Honcharenko, M. Bollmark, U. Tedebark and R. Strömberg, *ACS Omega*, 2021, **6**, 579–593.
18 N. Z. Fantoni, A. H. El-Sagheer and T. Brown, *Chem. Rev.*, 2021, **121**, 7122–7154.
19 S. I. Presolski, V. P. Hong and M. G. Finn, *Curr. Protoc. Chem. Biol.*, 2011, **3**, 153–162.
20 J. E. Hein and V. V. Fokin, *Chem. Soc. Rev.*, 2010, **39**, 1302–1315.
21 V. O. Rodionov, V. V. Fokin and M. G. Finn, *Angew. Chem., Int. Ed.*, 2005, **44**, 2210–2215.
22 B. T. Worrell, J. A. Malik and V. V. Fokin, *Science*, 2013, **340**, 457–460.
23 B. F. Straub, *Chem. Commun.*, 2007, 3868–3870, DOI: 10.1039/B706926J.
24 M. Ahlquist and V. V. Fokin, *Organometallics*, 2007, **26**, 4389–4391.
25 A. K. Gupta and A. Orthaber, *Chem. – Eur. J.*, 2018, **24**, 7536–7559.
26 M. G. Finn and V. V. Fokin, in *Catalysis without Precious Metals*, 2010, pp. 235–260. DOI: 10.1002/9783527631582.ch10.
27 V. O. Rodionov, S. I. Presolski, D. Díaz Díaz, V. V. Fokin and M. G. Finn, *J. Am. Chem. Soc.*, 2007, **129**, 12705–12712.
28 P. S. Donnelly, S. D. Zanatta, S. C. Zammit, J. M. White and S. J. Williams, *Chem. Commun.*, 2008, 2459–2461, DOI: 10.1039/B719724A.
29 R. Berg, J. Straub, E. Schreiner, S. Mader, F. Rominger and B. F. Straub, *Adv. Synth. Catal.*, 2012, **354**, 3445–3450.
30 A. Makarem, R. Berg, F. Rominger and B. F. Straub, *Angew. Chem., Int. Ed.*, 2015, **54**, 7431–7435.
31 A. W. Cook, Z. R. Jones, G. Wu, S. L. Scott and T. W. Hayton, *J. Am. Chem. Soc.*, 2018, **140**, 394–400.
32 C. Dong, R.-W. Huang, A. Sagadevan, P. Yuan, L. Gutiérrez-Arzaluz, A. Ghosh, S. Nematulloev, B. Alamer, O. F. Mohammed, I. Hussain, M. Rueping and O. M. Bakr, *Angew. Chem., Int. Ed.*, 2023, **62**, e202307140.
33 Y. Fang, K. Bao, P. Zhang, H. Sheng, Y. Yun, S.-X. Hu, D. Astruc and M. Zhu, *J. Am. Chem. Soc.*, 2021, **143**, 1768–1772.
34 J.-P. Gao, F.-Q. Zhang and X.-M. Zhang, *Adv. Sci.*, 2024, 2400377.
35 J. T. Petty, J. Zheng, N. V. Hud and R. M. Dickson, *J. Am. Chem. Soc.*, 2004, **126**, 5207–5212.
36 J. McNulty and K. Keskar, *Eur. J. Org. Chem.*, 2012, **2012**, 5462–5470.
37 O. A. Yeshchenko, I. M. Dmitruk, A. A. Alexeenko, M. Y. Losytskyy, A. V. Kotko and A. O. Pinchuk, *Phys. Rev. B: Condens. Matter Mater. Phys.*, 2009, **79**, 235438.
38 D. Schultz, K. Gardner, S. S. R. Oemrawsingh, N. Markešević, K. Olsson, M. Debord, D. Bouwmeester and E. Gwinn, *Adv. Mater.*, 2013, **25**, 2797–2803.
39 A. Gonzàlez-Rosell, C. Cerretani, P. Mastracco, T. Vosch and S. M. Copp, *Nanoscale Adv.*, 2021, **3**, 1230–1260.
40 C. I. Richards, S. Choi, J.-C. Hsiang, Y. Antoku, T. Vosch, A. Bongiorno, Y.-L. Tzeng and R. M. Dickson, *J. Am. Chem. Soc.*, 2008, **130**, 5038–5039.

41 H. C. Yeh, J. Sharma, J. J. Han, J. S. Martinez and J. H. Werner, *Nano Lett.*, 2010, **10**, 3106–3110.
42 J. T. Petty, D. Lewis, S. Carnahan, D. Kim and C. Couch, *J. Phys. Chem. B*, 2022, **126**, 3822–3830.
43 J. T. Petty, S. Carnahan, D. Kim and D. Lewis, *J. Chem. Phys.*, 2021, **154**, 244302.
44 C. J. Setzler, C. A. Arrington, D. Lewis and J. T. Petty, *J. Phys. Chem. B*, 2023, **127**, 10851–10860.
45 D. Lewis, C. Setzler, P. M. Goodwin, K. Thomas, M. Branham, C. A. Arrington and J. T. Petty, *J. Phys. Chem. C*, 2023, **127**, 10574–10584.
46 C. S. McKay and M. G. Finn, *Chem. Biol.*, 2014, **21**, 1075–1101.
47 V. A. Bloomfield, D. M. Crothers and I. Tinoco Jr., *Nucleic Acids: Structures, Properties, and Functions*, University Science Books, Sausaltio, CA, 2000.
48 G. A. Crosby and J. N. Demas, *J. Phys. Chem.*, 1971, **75**, 991–1024.
49 C. He, P. M. Goodwin, A. I. Yunus, R. M. Dickson and J. T. Petty, *J. Phys. Chem. C*, 2019, **123**, 17588–17597.
50 J. T. Petty, M. Ganguly, A. I. Yunus, C. He, P. M. Goodwin, Y.-H. Lu and R. M. Dickson, *J. Phys. Chem. C*, 2018, **122**, 28382–28392.
51 S. M. Copp, P. Bogdanov, M. Debord, A. Singh and E. Gwinn, *Adv. Mater.*, 2014, **26**, 5839–5845.
52 B. Sengupta, C. M. Ritchie, J. G. Buckman, K. R. Johnsen, P. M. Goodwin and J. T. Petty, *J. Phys. Chem. C*, 2008, **112**, 18776–18782.
53 K. Koszinowski and K. Ballweg, *Chem. – Eur. J.*, 2010, **16**, 3285–3290.
54 J. T. Petty, O. O. Sergev, M. Ganguly, I. J. Rankine, D. M. Chevrier and P. Zhang, *J. Am. Chem. Soc.*, 2016, **138**, 3469–3477.
55 S. M. Copp, D. Schultz, S. Swasey, J. Pavlovich, M. Debord, A. Chiu, K. Olsson and E. Gwinn, *J. Phys. Chem. Lett.*, 2014, **5**, 959–963.
56 J. T. Petty, O. O. Sergev, D. A. Nicholson, P. M. Goodwin, B. Giri and D. R. McMullan, *Anal. Chem.*, 2013, **85**, 9868–9876.
57 M. Ganguly, C. Bradsher, P. Goodwin and J. T. Petty, *J. Phys. Chem. C*, 2015, **119**, 27829–27837.
58 D. J. E. Huard, A. Demissie, D. Kim, D. Lewis, R. M. Dickson, J. T. Petty and R. L. Lieberman, *J. Am. Chem. Soc.*, 2019, **141**, 11465–11470.
59 L. D. Pachón, J. H. van Maarseveen and G. Rothenberg, *Adv. Synth. Catal.*, 2005, **347**, 811–815.
60 J. Belloni, M. Mostafavi, H. Remita, J.-L. Marignier and A. Marie-Odile Delcourt, *New J. Chem.*, 1998, **22**, 1239–1255.
61 N. M. Dimitrijevic, D. M. Bartels, C. D. Jonah, K. Takahashi and T. Rajh, *J. Phys. Chem. B*, 2001, **105**, 954–959.
62 B. G. Ershov, E. Janata, A. Henglein and A. Fojtik, *J. Phys. Chem.*, 1993, **97**, 4589–4594.
63 M. L. Rodríguez-Sánchez, M. J. Rodríguez, M. C. Blanco, J. Rivas and M. A. López-Quintela, *J. Phys. Chem. B*, 2005, **109**, 1183–1191.
64 S. A. Mitchell, G. A. Kenney-Wallace and G. A. Ozin, *J. Am. Chem. Soc.*, 1981, **103**, 6030–6035.
65 V. O. Rodionov, S. I. Presolski, S. Gardinier, Y.-H. Lim and M. G. Finn, *J. Am. Chem. Soc.*, 2007, **129**, 12696–12704.
66 F. David, C. Setzler, A. Sorescu, R. L. Lieberman, F. Meilleur and J. T. Petty, *J. Phys. Chem. Lett.*, 2022, **13**, 11317–11322.
67 E. Boz and N. Ş. Tüzün, *Dalton Trans.*, 2016, **45**, 5752–5764.
68 W. Wang, X.-Y. Zhai and L. Zhao, *Inorg. Chem.*, 2023, **62**, 1414–1422.
69 R. Berg and B. F. Straub, *Beilstein J. Org. Chem.*, 2013, **9**, 2715–2750.
70 V. Rück, V. A. Neacşu, M. B. Liisberg, C. B. Mollerup, P. H. Ju, T. Vosch, J. Kondo and C. Cerretani, *Adv. Opt. Mater.*, 2024, **12**, 2301928.
71 V. Rück, N. K. Mishra, K. K. Sørensen, M. B. Liisberg, A. B. Sloth, C. Cerretani, C. B. Mollerup, A. Kjaer, C. Lou, K. J. Jensen and T. Vosch, *J. Am. Chem. Soc.*, 2023, **145**, 16771–16777.
72 C. Cerretani, H. Kanazawa, T. Vosch and J. Kondo, *Angew. Chem., Int. Ed.*, 2019, **58**, 17153–17157.
73 J. T. Petty, M. Ganguly, I. J. Rankine, D. M. Chevrier and P. Zhang, *J. Phys. Chem. C*, 2017, **121**, 14936–14945.
74 M. S. Blevins, D. Kim, C. M. Crittenden, S. Hong, H.-C. Yeh, J. T. Petty and J. S. Brodbelt, *ACS Nano*, 2019, **13**, 14070–14079.
75 Y. Zhang, C. He, J. T. Petty and B. Kohler, *J. Phys. Chem. Lett.*, 2020, **11**, 8958–8963.